

Equivariant Networks for Porous Crystalline Materials

Marko Petkovic^{1,2[0009-0000-4918-6027]}, Pablo Romero Marimon^{1[0000-0001-9164-6541]}, Vlado Menkovski^{1,2[0000-0001-5262-0605]}, and Sofia Calero^{1,2[0000-0001-9535-057X]}

¹ Eindhoven University of Technology, Eindhoven, The Netherlands
`{m.petkovic1, v.menkovski, s.calero}@tue.nl`
`p.romero.marimon@student.tue.nl`

² Eindhoven Artificial Intelligence Systems Institute, Het Kranenveld 12, Eindhoven, The Netherlands

Abstract. Efficiently predicting properties of porous crystalline materials has great potential to accelerate the high throughput screening process for developing new materials, as simulations carried out using first principles model are often computationally expensive. To effectively make use of Deep Learning methods to model these materials, we need to utilize the symmetries present in the crystals, which are defined by their space group. Existing methods for crystal property prediction either have symmetry constraints that are too restrictive or only incorporate symmetries between unit cells. In addition, these models do not explicitly model the porous structure of the crystal. In this paper, we develop a model which incorporates the symmetries of the unit cell of a crystal in its architecture and explicitly models the porous structure. We evaluate our model by predicting the heat of adsorption of CO₂ for different configurations of the mordenite zeolite. Our results confirm that our method performs better than existing methods for crystal property prediction and that the inclusion of pores results in a more efficient model.

Keywords: Graph Neural Networks · Porous Materials · Equivariance.

1 Introduction

Deep Learning has shown to be of great use in materials science, in tasks like property prediction and high-throughput screening of potential materials [3]. In these workflows, many materials are first simulated using first principles methods, such as Density Functional Theory (DFT) and classical simulation, such as Molecular Dynamics (MD), to find candidate materials to synthesize. However, these simulations are often computationally expensive and can take days or weeks to simulate a single new material. With deep learning it is possible to accelerate the process of finding suitable materials, by developing data-driven surrogate models. These models scale significantly better than first principle simulators and allow for efficient search of the space of potential candidates [26].

Graph Neural Network (GNN) architectures are commonly used for modeling molecules and materials [20] as these structures are effectively represented as a graph. However, general-purpose GNNs are too restrictive regarding the symmetries they incorporate or only incorporate part of the symmetries present in crystal structures.

To overcome these limitations, for crystalline materials, multiple GNN architectures have recently been proposed [1,13,23,31] that accurately predict the properties of materials. These methods are specific extensions of general-purpose GNN that preserve the geometric structure of the crystal in their data representation. Nevertheless, none of the proposed models explicitly encode any information regarding pores or do not make use of all the symmetries present in the crystal material representation. We hypothesize that model architectures that do not explicitly model the porous structure of porous materials will struggle to infer the relevance of atom arrangements around pores for different properties.

Zeolites are a type of porous, crystalline materials, which are of particular interest, as they are easily synthesizable [14]. They are used in applications such as ion exchange and gas separation, and are a potential method for carbon capture [25]. The crystal structure of zeolites entirely consists of TO_4 tetrahedra. In these tetrahedra, the T-atoms can either be aluminium or silicon, and both have different influences on the properties of the material. All four corners of the tetrahedra are shared, which results in a porous material. In Figure 1, the porous structure of the mordenite zeolite can be seen. The ability to capture CO_2 of a zeolite can be measured by its heat of adsorption in kJ/mol and is calculated using Equation 1. Here, ΔU is the difference in internal energy before and after adsorption, R is the universal gas constant, and T is the temperature. The heat of adsorption can be influenced by the structure of the different types of zeolites, as well as the amount and distribution of aluminium atoms in the framework [2,17,32]. If aluminium atoms are present in a framework, cations such as sodium are added to balance the charge. Due to the presence of aluminium and sodium cations, the ability of the material to adsorb CO_2 increases. However, at the same time, the capacity of the material decreases, as the sodium cations occupy space in the pores where CO_2 could be adsorbed. It is unclear which distributions of aluminium and silicon in different zeolites are optimal to maximize the heat of adsorption.

$$-\Delta H = \Delta U - RT \quad (1)$$

In this paper, we propose a novel GNN architecture that exploits information regarding the porous structure, as well as the symmetry of these materials, using parameter sharing based on their space groups. This model allows us to effectively model the properties of porous crystalline materials.

We empirically validate our approach by modeling the heat of adsorption of CO_2 for the mordenite zeolite (MOR). Our contributions are threefold: 1) We adapt the Equivariant Crystal Networks (ECN) architecture from [13] to be equivariant with respect to the symmetry group of the unit cell. 2) We addi-

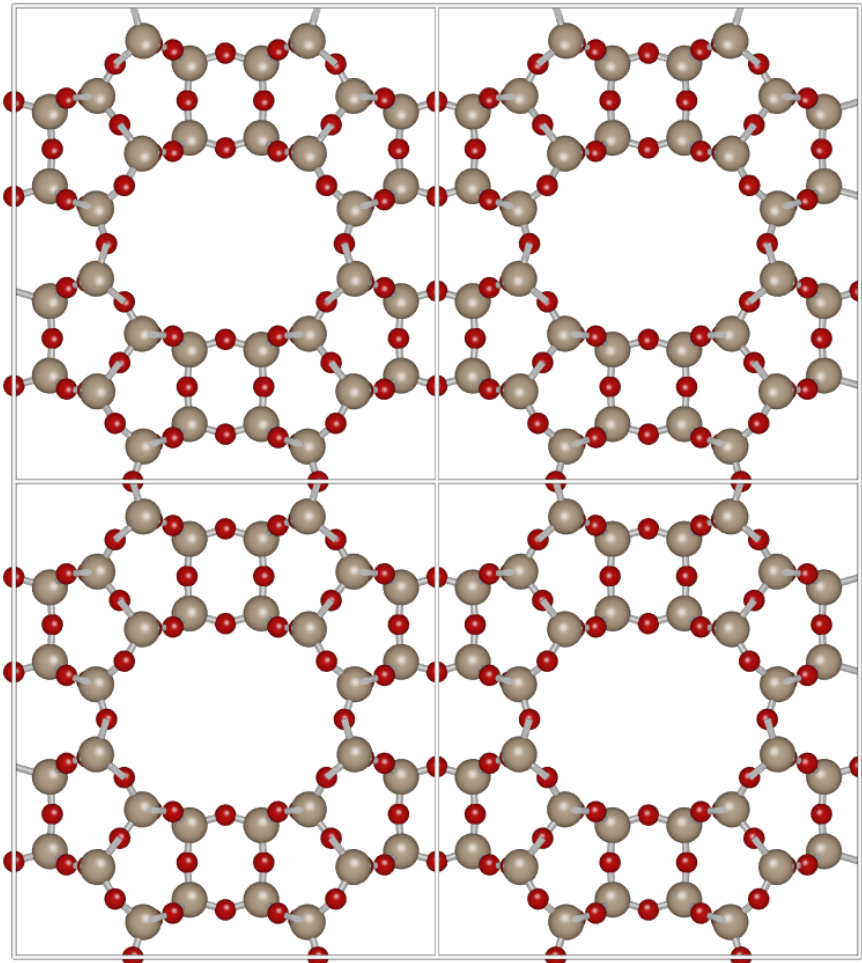


Fig. 1: Four unit cells of all silica mordenite viewed along the z-axis. Image generated using iRASPA [5].

tionally extend this architecture to explicitly model pores and show how this modification improves property prediction performance. 3) We introduce a new dataset containing different configurations of aluminium and silicon for the MOR zeolite, along with the CO_2 heat of adsorption values for the different configurations.

2 Related Work

Machine Learning Methods for Crystals Due to the success of different GNN architectures in modeling molecules, similar GNN architectures have been proposed for material data. Crystal Graph Convolutional Neural Networks (CGCNN) [31] are one of the first GNN architectures for crystals, which also include periodicity in the data representation and are invariant with respect to permutations of atomic indices. They can be seen as an extension of message passing [8] and graph convolutional networks [15]. In the MEGNet architecture [1], CGCNN is extended with a global state, that is used to improve generalization of the model. Continuous filter convolutions have been introduced in the SchNet architecture [22], which as a result can model the precise relative locations of atoms better when calculating local correlations. SchNet achieves invariance by pooling the final states of each atom. More recently a new approach has been proposed [13], which proposes a parameter-sharing scheme for message passing, based on the symmetry group of the crystal lattice. As such, the model gains in expressivity by encoding a part of the crystal symmetries in the model architecture.

Machine Learning in Porous Materials Existing ML methods for property prediction often make use of feature engineering, which traditional ML models or shallow neural networks use to predict properties of the material [12,33]. Another approach made use of the CGCNN architecture [28] and extended it with engineered features [29] to improve performance. In their method, nodes in the graph representation do not correspond to atoms but rather correspond to secondary building units (SBUs), which consist of multiple atoms.

3 Crystal Symmetries

In this section, we provide a brief summary of crystal symmetries based on [13] and show how we extend these to our case of porous crystalline materials.

Unit Cell Zeolites are crystalline materials, meaning that they contain an infinitely repeating pattern in all directions. This repeating pattern be described by the set of integral combinations of linearly independent lattice basis vectors \mathbf{a}_i :

$$A = \left\{ \sum_i^3 m_i \mathbf{a}_i \mid m_i \in \mathbb{Z} \right\} \quad (2)$$

The crystal lattice has an associated translation group T_A , which captures translational symmetry. A unit cell is a subset of the lattice, which tiles the space of the crystal when translated by lattice vectors and is the minimum repeating pattern of the crystal. The unit cell is defined by the basis vectors as follows:

$$U = \left\{ \sum_i^3 x_i \mathbf{a}_i \mid 0 \leq x_i < 1 \right\} \quad (3)$$

The unit cell of a crystalline material contains a set of atomic positions, which is defined as $S = \{\mathbf{x}_i \mid \mathbf{x}_i \in U\}$, where \mathbf{x}_i is the position of the atom in the unit cell. In addition to the set of atomic positions, we also define the set of pores contained in the unit cell. We define each pore using the atoms directly surrounding the pore. We represent each pore by the location of its center, as well as its surface area along which diffusion happens in terms of \AA^2 . This results in the following set of pores: $P = \{(\mathbf{x}_{p_i}, \text{area}(p_i)) \mid p_i \in U\}$, where p_i is the pore and \mathbf{x}_{p_i} is the centre of the pore.

Space Groups In crystalline materials, there are often multiple symmetries present inside the unit cell, defined by a space group G . The space group G is the set of isometries that maps the crystal structure onto itself. Each element of the space group can be expressed as a linear transformation \mathbf{W} and a translation \mathbf{t} , represented by a tuple (\mathbf{W}, \mathbf{t}) . When mapping a vector \mathbf{x} using an element of the space group, it is mapped to $\mathbf{W}\mathbf{x} + \mathbf{t}$.

Inside a unit cell, every element of the space group G maps the atomic positions and the positions of the pores in the unit cell onto itself. While the type of atom at a certain position in the unit cell might change as a result of a transformation, the material remains the same. Therefore, each group action g of the space group can be considered a permutation of the atoms and pores in the unit cell.

Group Orbits By applying all the different elements of a space group G to an element, we create the orbit of an element. In case the element is a vector \mathbf{x} , its orbit is the set of vectors that the element can be moved to by the group action. The orbit of \mathbf{x} is defined as follows:

$$G \cdot \mathbf{x} = \{g \cdot \mathbf{x} \mid g \in G\} \quad (4)$$

4 Methods

Crystal Representation In our crystal representation, we only consider the set of atoms inside of the unit cell, as the content of a unit cell fully defines the porous structures and symmetry of the material. Each of the atoms in the unit cell is represented by a feature vector \mathbf{h}_i that is a one-hot encoding of the atom type. Next to this, we represent each pore inside the unit cell with a feature vector \mathbf{p}_i , which contains the surface area of the pore, as well as the number of atoms surrounding that pore.

To represent the topology of the atoms and pores we construct a graph, where each atom is represented with a node, then in case the crystal contains clearly defined covalent bonds these are represented as edges in the graph. Otherwise, the edges are drawn between atoms that share a Voronoi face and are sufficiently close to each other [11].

Finally, to include the pore nodes we add additional edges between the pore nodes and each atom on the boundary of the pore. In case multiple pores are

intersecting, additional nodes are included where the pores intersect and are connected to each other in the graph. By including pore nodes, all atoms around the same pore are reachable from each other at most in two steps. Without pore nodes, this number could have been significantly larger, particularly for crystals with larger pores.

The notion of a pore has a certain analogy to the global feature vector introduced in MEGNet [1]. However, our approach is distributed in the geometry of the crystal which in turn allows the GNN-based model to learn locally distributed features, which is a more parameter-efficient solution.

Based on [22], we make use of radial basis functions to encode the distance between two neighboring nodes in the graph. We calculate the edge embedding \mathbf{e}_{ij} as in Equation 5, where γ and μ are hyperparameters.

$$\mathbf{e}_{ij} = \exp(-\gamma(\|\mathbf{x}_i - \mathbf{x}_j\| - \mu)^2) \quad (5)$$

When calculating the distance between two atoms, we respect the periodic boundary conditions set by the unit cell by using the minimum image convention. Thus, we treat the opposite boundaries as a single boundary and consider the atoms and pores as neighbors and therefore sharing an edge.

Since we are creating and developing a network architecture to predict properties based on the silicon and aluminium configuration in mordenite (and zeolites in general), we do not explicitly encode the oxygen atoms as nodes, as only the atoms placed in the t-sites of each TO_4 tetrahedron can change.

Equivariant Message Passing Since the space group acts as a permutation on the atoms and pores in the unit cell, we can describe the action of a group element using Equation 6. Here, π_g^h and π_g^p are the permutations of the atoms and pores as a result of group action g .

$$(g\mathbf{h}_i = \mathbf{h}_{\pi_g^h(i)} \wedge g\mathbf{p}_j = \mathbf{p}_{\pi_g^p(j)}) \forall g \in G \quad (6)$$

As we model different configurations of the same crystal structure using our architecture, we need to create a model which is equivariant to G . The model we define is based on the message passing framework [8], which we extend by defining parameter sharing patterns [19] for the edge and node update functions.

First, we will define a parameter-sharing pattern for the graph without the pores. Following [13], we define the parameter sharing pattern as the colored bipartite graph $\Omega \equiv (\mathbb{N}, \alpha, \beta)$. Here, \mathbb{N} is the set of input atoms, α is the edge color function ($\alpha : \mathbb{N} \times \mathbb{N} \rightarrow \{1, \dots, C_e\}$) and β is the node color function ($\beta : \mathbb{N} \rightarrow \{1, \dots, C_h\}$). For the functions α and β , C_e and C_h are the amount of unique edge colors and node colors respectively. As shown in equations 7 and 8 the color functions take the same value if two edges or atoms lie on each others orbit.

$$\alpha(i, j) = \alpha(k, l) \iff (k, l) \in G \cdot (i, j) \quad (7)$$

$$\beta(i) = \beta(j) \iff j \in G \cdot i \quad (8)$$

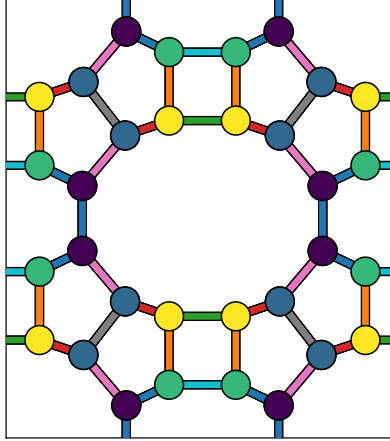


Fig. 2: Weight sharing scheme for mordenite without pore nodes, viewed along the z-axis. Nodes/edges that are the same color share parameters in their node/edge update functions. Note that in some edges 2 different sets of parameters are used, as in some cases sending a message from node i to j is not symmetric to sending a message from node j to i .

When introducing a parameter sharing pattern based on the edge and node coloring function, we are effectively introducing an additional edge (node) update function for each "unique" edge (node) in the graph representation of the crystal. As such, the model architecture is equivariant to the space group of the crystal, following Claim 6.1 from [13]. In Figure 2, an example of what the parameter sharing pattern for MOR looks like can be found, where nodes and edges are colored according to Equations 7 and 8. The message passing operation equivariant to the space group is defined as follows:

$$\mathbf{m}_{ij} = \phi_e^{\alpha(i,j)}(\mathbf{h}_i^t, \mathbf{h}_j^t, \mathbf{e}_{ij}), \quad (9)$$

$$\mathbf{m}_i = \frac{1}{|N_i|} \sum_{j \in N_i} \mathbf{m}_{ij}, \quad (10)$$

$$\mathbf{h}_i^{t+1} = \phi_h^{\beta(i)}(\mathbf{h}_i^t, \mathbf{m}_i^h), \quad (11)$$

To also include the pore nodes in \mathbb{N} , new colors are added to the coloring functions α and β , which are used for coloring the edges between pore nodes and atoms and the coloring of pore nodes. Since the space group does not change as a result of including the pore nodes in the graph, the colors of the edges between atoms and the colors of the atoms themselves remains the same. As a result, the model remains equivariant to the space group of the crystal. However, as new types of edges and nodes were introduced, the message passing operation changes. In Equations 12-19 we present the new message passing operations for crystal with non intersecting pores. In case of a more complex material with

intersecting pores, additional porous nodes should be inserted to represent the intersection. Furthermore, additional message and aggregation functions between two porous nodes should be defined and this information should also be used in the pore node update function.

To differentiate between messages sent between atoms and messages sent between atoms and pores, we use three types of messages: messages between atoms (Equation 12), messages sent from a node to an atom (Equation 13) and messages sent from an atom to a pore (Equation 14). Likewise, when performing the message aggregation step, we separately aggregate the different types of messages (Equations 15 - 17). Here, N_i^h is the set of neighbouring atoms for atom i , N_i^k is the set of neighbouring pores for atom i and N_i^l is the set of neighbouring atoms for pore i . Finally, we introduce separate node update functions for pores and atoms. The atom update function (Equation 18) receives the current embedding, as well as the aggregated messages from neighbouring atoms and pores. The pore update function (Equation 19) only uses the messages received from neighbouring atoms in addition to its own embedding.

$$\mathbf{m}_{ij}^h = \phi_e^{\alpha(i,j)}(\mathbf{h}_i^t, \mathbf{h}_j^t, \mathbf{e}_{ij}), \quad (12)$$

$$\mathbf{m}_{ij}^k = \phi_e^{\alpha(i,j)}(\mathbf{h}_i^t, \mathbf{p}_j^t, \mathbf{e}_{ij}), \quad (13)$$

$$\mathbf{m}_{ij}^l = \phi_e^{\alpha(i,j)}(\mathbf{p}_i^t, \mathbf{h}_j^t, \mathbf{e}_{ij}), \quad (14)$$

$$\mathbf{m}_i^h = \frac{1}{|N_i^h|} \sum_{j \in N_i^h} \mathbf{m}_{ij}^h, \quad (15)$$

$$\mathbf{m}_i^k = \frac{1}{|N_i^k|} \sum_{j \in N_i^k} \mathbf{m}_{ij}^k, \quad (16)$$

$$\mathbf{m}_i^l = \frac{1}{|N_i^l|} \sum_{j \in N_i^l} \mathbf{m}_{ij}^l, \quad (17)$$

$$\mathbf{h}_i^{t+1} = \phi_h^{\beta(i)}(\mathbf{h}_i^t, \mathbf{m}_i^h, \mathbf{m}_i^k), \quad (18)$$

$$\mathbf{p}_i^{t+1} = \phi_h^{\beta(i)}(\mathbf{p}_i^t, \mathbf{m}_i^l). \quad (19)$$

In both the equivariant message passing operations with and without pores, the message update functions (ϕ_e) are implemented as one layer MLPs with a global shared attention function [27]. The node update functions (ϕ_h) are implemented as two layer MLPs with a skip connection [10].

5 Experiments

Network Architecture As we are training the model on a single crystal structure, it suffices to keep the architecture relatively simple. We perform 6 message passing steps, with an embedding size for both edges and atoms (pores) of 8. Then, we process each atom (pore) with an MLP with an output size of 24. Following this, sum pooling is used to perform an invariant aggregation, which

is followed by a 2 layer MLP to make predictions. Our model implementation is based on [13] and uses the PyTorch [18] and PyTorch scattter [6] packages as well as the AutoEquiv library [24].

Data Generation For our dataset, we generated multiple mordenite frameworks with varying aluminium and silicon distributions, and calculated their corresponding CO₂ heat of adsorptions. For generating the structures, the zeoran program was used [21]. 4123 structures were generated, where each structure contains between 0 and 12 aluminium atoms, with the rest being silicon. The program makes use of four different algorithms, which places aluminium atoms in either random positions, chains, clusters or homogeneously throughout the zeolite framework. To calculate the CO₂ heat of adsorption Grand-Canonical Monte Carlo simulations were carried out using the Widom Particle Insertion method [30], performed with the RASPA software [4]. Frameworks were considered rigid and the force field parameters for the interactions between the zeolite and the adsorbate were taken from [7]. The force field for carbon dioxide was taken from [9].

In Figure 3a, the distribution of the heat of adsorption of the dataset is shown. While there is a strong correlation between the amount of aluminium atoms and the heat of adsorption, there is still significant variance in the heat of adsorption for each amount of aluminium substitutions (Figure 3b). As such, a more complex model is necessary to understand the influence of different configurations on the heat of adsorption.

Model Evaluation To evaluate the predictive performance and the ability of our models to generalize, we included configurations with up to 11 aluminium atoms (3778 datapoints) in the training set, and tested the model on configura-

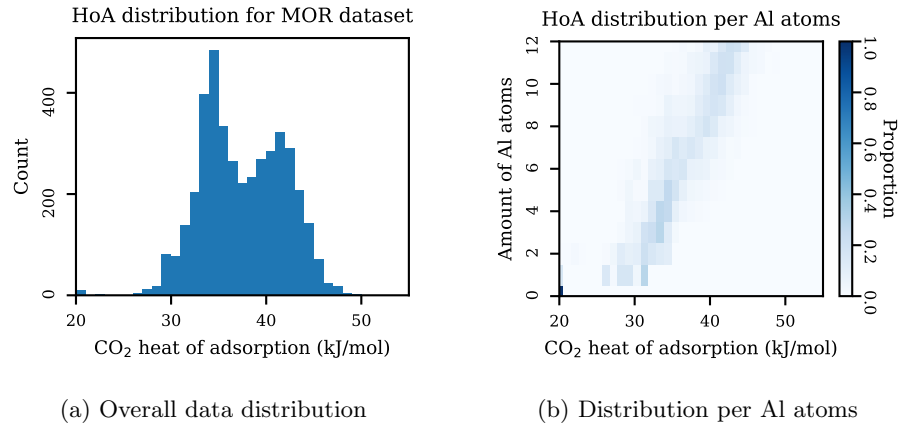


Fig. 3: CO₂ heat of adsorption distributions for MOR dataset

Table 1: Performance of different model architectures on CO₂ heat of adsorption prediction for the MOR dataset.

	MAE	MSE
CGCNN	1.618 \pm 0.112	4.511 \pm 0.493
MEGNet	1.397 \pm 0.062	3.627 \pm 0.241
SchNet	1.123 \pm 0.059	2.227 \pm 0.189
Ours (without pores)	1.378 \pm 0.136	3.158 \pm 0.521
Ours (with pores)	1.002 \pm 0.032	1.742 \pm 0.099

tions with 12 aluminium atoms (345 datapoints). We compare the performance of our model with and without pores to different baselines [11,22,31]. For the different baselines we also make use of 6 message passing/interaction steps, and use hidden sizes of 8, with the final MLP having 24 nodes.

Since predicting the heat of adsorption is a regression task, we made use of the Huber loss function when training. We used the AdamW optimizer [16] with a learning rate of 0.001, and trained each model for 200 epochs. We report the mean-absolute error (MAE) and mean-squared error (MSE). To obtain confidence bounds for the errors, we trained each model 10 times with different random initializations of the weights. The code for the model implementations and the mordenite dataset are available on github.com/marko-petkovic/porousequivariantnetworks.

As can be seen in Table 1, our model with pores obtains significantly better results than the model without pores, as well as the different architectures. We speculate that the improved results are due to the explicit modeling of the porous structure of the material. In Figure 5 the predictions by our best performing model are plotted against the true heat of adsorption values, showing that the predictions are mostly accurate, and that the model is able to generalize beyond

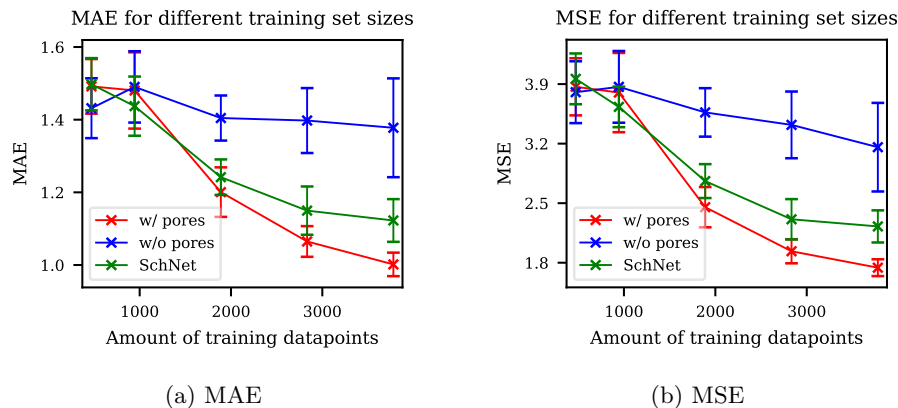


Fig. 4: Error on test set with different amounts of training data

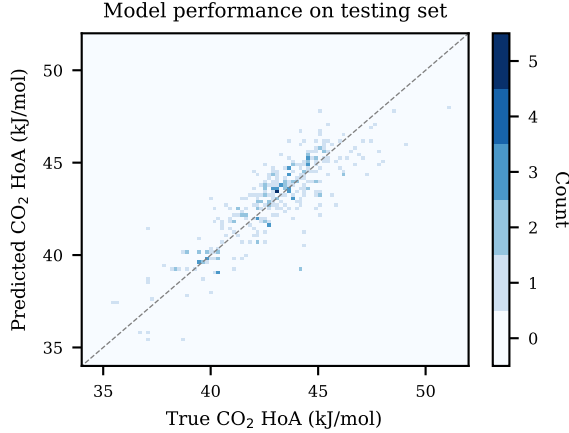


Fig. 5: Predicted heat of adsorption plotted against the true heat of adsorption for the best performing model with pores on the test set

the training data. The SchNet architecture obtains the second best results, likely due to the spatial continuous filters being able to implicitly model a part of the porous structure. Our model without pores performs on a similar level as MEGNet. A likely explanation for the better performance than CGCNN is that both models use additional information (symmetries and maintaining a global state respectively).

In addition, we also carried out experiments to compare the data efficiency of our model with pores, without pores and SchNet. Here, we trained each model using different fractions ($\frac{1}{8}, \frac{1}{4}, \frac{1}{2}, \frac{3}{4}$ and 1) of the training set, and evaluated them on the same testing set. In Figure 4 we see that as the amount of training data increases, the model with pores and SchNet are improving its performance more than the model without pores. The model with pores is slightly more efficient than SchNet, but the difference is not significant for smaller amounts of training data. The inclusion of pore nodes likely helps the model to understand the influence of the distribution of aluminium atoms with less data.

6 Discussion

We have proposed a new type of network which can exploit both symmetries inside the unit cell as well as the structure of porous, crystalline materials. Our method achieved excellent performance on the CO₂ heat of adsorption prediction task, and has also shown a better data efficiency. This class of models has a significant potential to accelerate the high throughput screening of porous materials, by quickly narrowing the search space for candidate materials. A drawback of our method is the inability to train the model on multiple crystals at the same time. A potential direction for future research could be to base the parameter

sharing on SBUs of zeolites or metal organic frameworks, as multiple structures share the same SBUs. This way, increased expressivity of the parameter sharing idea is retained, while the model can generalize beyond a single type of crystal.

References

1. Chen, C., Ye, W., Zuo, Y., Zheng, C., Ong, S.P.: Graph networks as a universal machine learning framework for molecules and crystals. *Chemistry of Materials* **31**(9), 3564–3572 (2019)
2. Choi, H.J., Jo, D., Hong, S.B.: Effect of framework si/al ratio on the adsorption mechanism of co₂ on small-pore zeolites: Ii. merlinoite. *Chemical Engineering Journal* **446**, 137100 (2022)
3. Choudhary, K., DeCost, B., Chen, C., Jain, A., Tavazza, F., Cohn, R., Park, C.W., Choudhary, A., Agrawal, A., Billinge, S.J., et al.: Recent advances and applications of deep learning methods in materials science. *npj Computational Materials* **8**(1), 59 (2022)
4. Dubbeldam, D., Calero, S., Ellis, D.E., Snurr, R.Q.: Raspa: molecular simulation software for adsorption and diffusion in flexible nanoporous materials. *Molecular Simulation* **42**(2), 81–101 (2016)
5. Dubbeldam, D., Calero, S., Vlugt, T.J.: iraspa: Gpu-accelerated visualization software for materials scientists. *Molecular Simulation* **44**(8), 653–676 (2018)
6. Fey, M.: Pytorch scatter (2023)
7. Garcia-Sanchez, A., Ania, C.O., Parra, J.B., Dubbeldam, D., Vlugt, T.J., Krishna, R., Calero, S.: Transferable force field for carbon dioxide adsorption in zeolites. *The Journal of Physical Chemistry C* **113**(20), 8814–8820 (2009)
8. Gilmer, J., Schoenholz, S.S., Riley, P.F., Vinyals, O., Dahl, G.E.: Neural message passing for quantum chemistry. In: International conference on machine learning. pp. 1263–1272. PMLR (2017)
9. Harris, J.G., Yung, K.H.: Carbon dioxide's liquid-vapor coexistence curve and critical properties as predicted by a simple molecular model. *The Journal of Physical Chemistry* **99**(31), 12021–12024 (1995)
10. He, K., Zhang, X., Ren, S., Sun, J.: Deep residual learning for image recognition. In: Proceedings of the IEEE conference on computer vision and pattern recognition. pp. 770–778 (2016)
11. Isayev, O., Oses, C., Toher, C., Gossett, E., Curtarolo, S., Tropsha, A.: Universal fragment descriptors for predicting properties of inorganic crystals. *Nature communications* **8**(1), 15679 (2017)
12. Jablonka, K.M., Ongari, D., Moosavi, S.M., Smit, B.: Big-data science in porous materials: materials genomics and machine learning. *Chemical reviews* **120**(16), 8066–8129 (2020)
13. Kaba, S.O., Ravanbakhsh, S.: Equivariant networks for crystal structures. In: Advances in Neural Information Processing Systems (2022)
14. Khaleque, A., Alam, M.M., Hoque, M., Mondal, S., Haider, J.B., Xu, B., Johir, M., Karmakar, A.K., Zhou, J., Ahmed, M.B., et al.: Zeolite synthesis from low-cost materials and environmental applications: A review. *Environmental Advances* **2**, 100019 (2020)
15. Kipf, T.N., Welling, M.: Semi-supervised classification with graph convolutional networks. *arXiv preprint arXiv:1609.02907* (2016)

16. Loshchilov, I., Hutter, F.: Decoupled weight decay regularization. arXiv preprint arXiv:1711.05101 (2017)
17. Moradi, H., Azizpour, H., Bahmanyar, H., Rezamandi, N., Zahedi, P.: Effect of si/al ratio in the faujasite structure on adsorption of methane and nitrogen: a molecular dynamics study. *Chemical Engineering & Technology* **44**(7), 1221–1226 (2021)
18. Paszke, A., Gross, S., Massa, F., Lerer, A., Bradbury, J., Chanan, G., Killeen, T., Lin, Z., Gimelshein, N., Antiga, L., et al.: Pytorch: An imperative style, high-performance deep learning library. *Advances in neural information processing systems* **32** (2019)
19. Ravanbakhsh, S., Schneider, J., Poczos, B.: Equivariance through parameter-sharing. In: International conference on machine learning. pp. 2892–2901. PMLR (2017)
20. Reiser, P., Neubert, M., Eberhard, A., Torresi, L., Zhou, C., Shao, C., Metni, H., van Hoesel, C., Schopmans, H., Sommer, T., et al.: Graph neural networks for materials science and chemistry. *Communications Materials* **3**(1), 93 (2022)
21. Romero-Marimon, P.: Zeoran (3 2023), <https://github.com/promerma/zeoran>
22. Schütt, K., Kindermans, P.J., Sauceda Felix, H.E., Chmiela, S., Tkatchenko, A., Müller, K.R.: Schnet: A continuous-filter convolutional neural network for modeling quantum interactions. *Advances in neural information processing systems* **30** (2017)
23. Schütt, K.T., Sauceda, H.E., Kindermans, P.J., Tkatchenko, A., Müller, K.R.: Schnet—a deep learning architecture for molecules and materials. *The Journal of Chemical Physics* **148**(24), 241722 (2018)
24. Shakerinava, M.: Autoequiv (2 2021), <https://github.com/mshakerinava/AutoEquiv>
25. Sneddon, G., Greenaway, A., Yiu, H.H.: The potential applications of nanoporous materials for the adsorption, separation, and catalytic conversion of carbon dioxide. *Advanced Energy Materials* **4**(10), 1301873 (2014)
26. Stein, H.S., Gregoire, J.M.: Progress and prospects for accelerating materials science with automated and autonomous workflows. *Chemical science* **10**(42), 9640–9649 (2019)
27. Veličković, P., Cucurull, G., Casanova, A., Romero, A., Lio, P., Bengio, Y.: Graph attention networks. arXiv preprint arXiv:1710.10903 (2017)
28. Wang, R., Zhong, Y., Bi, L., Yang, M., Xu, D.: Accelerating discovery of metal–organic frameworks for methane adsorption with hierarchical screening and deep learning. *ACS Applied Materials & Interfaces* **12**(47), 52797–52807 (2020)
29. Wang, R., Zou, Y., Zhang, C., Wang, X., Yang, M., Xu, D.: Combining crystal graphs and domain knowledge in machine learning to predict metal-organic frameworks performance in methane adsorption. *Microporous and Mesoporous Materials* **331**, 111666 (2022)
30. Widom, B.: Some topics in the theory of fluids. *The Journal of Chemical Physics* **39**(11), 2808–2812 (1963)
31. Xie, T., Grossman, J.C.: Crystal graph convolutional neural networks for an accurate and interpretable prediction of material properties. *Physical review letters* **120**(14), 145301 (2018)
32. Yang, C.T., Janda, A., Bell, A.T., Lin, L.C.: Atomistic investigations of the effects of si/al ratio and al distribution on the adsorption selectivity of n-alkanes in brønsted-acid zeolites. *The Journal of Physical Chemistry C* **122**(17), 9397–9410 (2018)

33. Zhang, C., Xie, Y., Xie, C., Dong, H., Zhang, L., Lin, J.: Accelerated discovery of porous materials for carbon capture by machine learning: A review. *MRS Bulletin* **47**(4), 432–439 (2022)

A Ethical Statement

As this work is about material property prediction, no personal data has been collected or processed, and the proposed models cannot infer any personal data. In this work, we propose an architecture for modeling porous materials. Improving these materials with insights gained from ML can result in materials better at tasks like carbon capture or gas separation, and can thus only serve to improve environmental well-being. As such, we do not believe there are any ethical implications related to this work.